

# Synthesis and Analysis of Entangled Photonic Qubits in Spatial-Parity Space

Timothy Yarnall,<sup>1</sup> Ayman F. Abouraddy,<sup>2</sup> Bahaa E. A. Saleh,<sup>1</sup> and Malvin C. Teich<sup>1,\*</sup>

<sup>1</sup>*Quantum Imaging Laboratory, Departments of Electrical & Computer Engineering and Physics,  
Boston University, Boston, Massachusetts 02215-2421, USA*

<sup>2</sup>*Research Laboratory of Electronics, Massachusetts Institute of Technology, Cambridge, Massachusetts 02139-4307, USA*  
(Dated: February 5, 2008)

We present the novel embodiment of a photonic qubit that makes use of one continuous spatial degree of freedom of a single photon and relies on the the *parity* of the photon's transverse spatial distribution. Using optical spontaneous parametric downconversion to produce photon pairs, we demonstrate the controlled generation of entangled-photon states in this new space. Specifically, two Bell states, and a continuum of their superpositions, are generated by simple manipulation of a classical parameter, the optical-pump spatial parity, and not by manipulation of the entangled photons themselves. An interferometric device, isomorphic in action to a polarizing beam splitter, projects the spatial-parity states onto an even-odd basis. This new physical realization of photonic qubits could be used as a foundation for future experiments in quantum information processing.

PACS numbers: 42.65.Lm, 03.65.Ud, 03.67.Mn

The generation of entangled states is the cornerstone of experimental quantum information science [1]. Photonic entangled systems are of particular interest because of their importance for quantum cryptography [2] and quantum computation with linear optics [3]. The physical realization of photonic states has hitherto taken the form of *discrete* degrees of freedom (predominantly in the form of qubits) such as polarization [4] and time-energy bins [5]. While the *continuous* spatial degrees of freedom of entangled photons have been the subject of considerable interest [6], this feature has heretofore been only partially harnessed for quantum information processing. One approach to endowing the spatial degrees of freedom of a photon with a qubit or a qudit structure is a discretization of the spatial domain by making use of slits or pinholes [7]. Another method begins by adopting either the Hermite-Gaussian [8] or Laguerre-Gaussian modes [9] as a basis for describing a photon's *two-dimensional* transverse distribution. Typically only two of the initially infinite number of modes are retained, via filtering or post-selection, to serve as qubit levels, resulting in a *truncation* of the Hilbert space. Another approach relies on so-called *pseudo-spin* operators that have been studied using photon-number Fock states [10]; however, the experimental realization of the proposed schemes has not been forthcoming, undoubtedly due to the difficulty of preparing and manipulating Fock states [11]. The pseudo-spin approach relies on *mapping* (not filtering or truncating) a Hilbert space associated with a continuous variable onto a discrete smaller-dimensional space, in particular a two-dimensional (2D) one [10], to achieve a qubit structure *without truncating* the initial Hilbert space.

In this Letter, we present a new physical embodiment of photonic *qubits* that makes use of a *one-dimensional* (1D) continuous spatial degree of freedom of single photons that is readily implemented experimentally with-

out discretization or truncation. We generate entangled photonic qubits in this new Hilbert space using the accessible process of optical spontaneous parametric downconversion (SPDC) *without* spatial filtering. Each qubit is encoded in the spatial parity (even-odd) of the photon's *one-dimensional* transverse modes and is a realization of the pseudo-spin approach in the spatial domain. The mathematical underpinning of this approach relies on the isomorphism between the *single-mode multi-photon* quantization and the *single-photon multi-mode* quantization of the electromagnetic field that has recently led to the concept of parity entanglement, as identified theoretically in Ref. [12]. The infinite-dimensional Hilbert space of *one* spatial degree of freedom for each photon is thereby mapped onto a 2D Hilbert space describing its spatial-parity qubit. It is notable that an additional qubit may be encoded in an identical manner on the orthogonal transverse dimension because  $x$  and  $y$  are on equal footing as spatial coordinates. This creates a sharp distinction from approaches based on orbital angular momentum, which rely on an angular degree of freedom in a polar coordinate system; encoding an additional qubit in the radial variable would require a radically different approach.

We begin by discussing the construction of operators on the spatial-parity space, which are strikingly simple to implement, thus making this approach an attractive alternative to other physical realizations of photonic qubits. This is highlighted in Fig. 1, where comparison is drawn between the familiar devices that manipulate polarization qubits, as an archetypical realization of a photonic qubit, and their isomorphic counterparts in 1D spatial-parity space (see Ref. [12] for a detailed analysis). The 2D manifold of pure states of polarization (spatial parity) can be represented by the surface of a Poincaré sphere with the horizontal  $|H\rangle$  (even,  $|e\rangle$ ) and vertical  $|V\rangle$  (odd,  $|o\rangle$ ) states located at antipodes. (Any qubit can,

of course, be represented by the surface of a Poincaré sphere; consider, for example, Ref. [13], in which this treatment is applied to classical light in first-order Gaussian modes after truncating all other modes.) The Pauli operator  $\sigma_x$  in polarization space is a half-wave plate rotated by  $45^\circ$  with respect to  $|H\rangle$ , while its pseudo-spin counterpart in parity space is a simple phase plate that introduces a phase shift of  $\pi$  between the two halves of the plane (a parity flipper, PF). The Pauli operator  $\sigma_z$  in polarization space is a half-wave plate, while its pseudo-spin counterpart in parity space is a spatial flipper (SF), a device that flips the beam in space  $\phi(x) \rightarrow \phi(-x)$ , which may be implemented with a mirror, for example.

With these building blocks in hand, we construct some operators essential for quantum information processing. A rotation  $\mathbf{R}(\theta)$  in polarization space is implemented by a polarization rotator, for example, and in parity space by a phase plate that introduces a phase  $\theta$  between the two half planes (a parity rotator, PR). An even beam  $|e\rangle$  incident on a phase plate with a  $\theta = \pi$  difference between the two halves (a PF) obviously becomes odd  $|o\rangle$ , and vice versa. Less obvious is the fact that introducing a phase difference  $\theta = \frac{\pi}{2}$  between the two halves of the plane of an even mode transforms it into the equal superposition  $\frac{1}{\sqrt{2}}\{|e\rangle + i|o\rangle\}$ . Finally, a polarizing beam splitter that projects the polarization state by separating the two orthogonal components into separate spatial paths has its counterpart in a parity analyzer (PA): this device is a balanced Mach-Zehnder interferometer (MZI) [14] with a SF placed in one arm that serves to separate the  $|e\rangle$  and  $|o\rangle$  components of an incoming state into two separate spatial paths. Thus quantum information processing experiments conducted on photonic qubits in polarization space may be readily implemented in 1D spatial-parity space using Fig. 1 as a Rosetta stone that guides the translation between these implementations. Previous work has identified similar devices for manipulating spatial parity [15], but without identifying the underlying qubit structure of the photon field.

In this Letter, we demonstrate the ability to control, in a precise manner, the generation of entangled two-photon states in parity space by manipulating a classical parameter: the pump spatial parity. The experimental arrangement is shown schematically in Fig. 2(a). A linearly polarized monochromatic pump laser diode (wavelength 405 nm, power 50 mW) with an even spatial profile illuminates a 1.5-mm-thick  $\beta$ -barium borate (BBO) nonlinear optical crystal (NLC) in a collinear type-I configuration (signal and idler photons have the same polarization, orthogonal to that of the pump), after passing through a phase plate that serves as a PR for the pump spatial parity. The pump is removed using a polarizing beam splitter placed after the crystal as well as by interference filters (centered at 810 nm, 10-nm bandwidth) placed in front of the detectors  $D_e$  and  $D_o$  (EG&G SPCM-AQR-15-FC), the outputs of which are fed to a coincidence

circuit (denoted  $\otimes$ ) and thence to a counter. The signal and idler photons are directed to a parity-sensitive MZI (PS-MZI), which, at a relative path delay  $\tau = 0$ , serves as a PA, as described above. For purposes of comparison, we also carry out all the experiments with the SF removed, corresponding to a traditional MZI.

It can be shown [12] that an even (odd) pump results in downconverted photonic qubits in a  $|\Phi^+\rangle$  ( $|\Psi^+\rangle$ ) parity state,

$$\begin{aligned} |\text{even}\rangle_p &\rightarrow |\text{even}\rangle_s |\text{even}\rangle_i + |\text{odd}\rangle_s |\text{odd}\rangle_i = |\Phi^+\rangle, \\ |\text{odd}\rangle_p &\rightarrow |\text{even}\rangle_s |\text{odd}\rangle_i + |\text{odd}\rangle_s |\text{even}\rangle_i = |\Psi^+\rangle, \end{aligned} \quad (1)$$

where p, s, and i refer to the pump, signal, and idler, respectively. Placing the PR in the pump beam results in the superposition  $\cos\theta|\text{even}\rangle_p + i\sin\theta|\text{odd}\rangle_p$ , where varying  $\theta$  traces out the great circle, indicated by the dashed arrow, on the surface of the Poincaré sphere in Fig. 1. The SPDC photons produced by such a pump are generated in the superposition state  $\cos\theta|\Phi^+\rangle + i\sin\theta|\Psi^+\rangle$ . An interesting consequence of controlling the pump parity in this fashion is that the two-photon state is guaranteed to remain *maximally entangled*; the concurrence  $C$  [16] of the state is always maximal ( $C = 1$ ) for all  $\theta$ . This is in contrast to using a pump in the superposition  $\cos\theta|\text{even}\rangle_p + \sin\theta|\text{odd}\rangle_p$ , where varying  $\theta$  traces out a different great circle on the surface of the Poincaré sphere, such that the concurrence  $C = |\cos 2\theta|$ , whereupon a *separable* state ( $C = 0$ ) is obtained when  $\theta = \frac{\pi}{4}$ .

Before presenting the experimental results, we provide a heuristic overview of the interference effects expected in this arrangement. The two entangled photons are incident at the same port of a beam splitter; two distinct cases arise, leading to qualitatively different interference patterns. In the first case, each photon emerges from a different beam-splitter port. When these photons are brought back at a second beam splitter, after a delay  $\tau$  in one of the arms (see Fig. 2), the well-known Hong-Ou-Mandel (HOM) [17] dip is observed in the coincidence rate  $G^{(2)}(\tau)$ . In the second case, the two photons emerge together from either output port of the first beam splitter. For SPDC with a monochromatic pump, the frequencies of the two photons are anti-correlated so that  $\omega_s = \frac{\omega_p}{2} + \Omega$  and  $\omega_i = \frac{\omega_p}{2} - \Omega$ , where  $\frac{\omega_p}{2}$  is half the pump frequency and  $\Omega$  is a deviation therefrom. A delay  $\tau$  will then lead to a fixed phase difference  $\exp\{-i(\frac{\omega_p}{2} + \Omega)\tau\} \exp\{-i(\frac{\omega_p}{2} - \Omega)\tau\} = \exp\{-i\omega_p\tau\}$  between the two paths, whereupon  $G^{(2)}(\tau)$  will simply be a sinusoid at the pump period  $T_{\text{pump}}$  [18]. These two cases coexist in the experimental arrangement shown in Fig. 2, resulting in a coincidence interferogram that combines the HOM dip and the sinusoid at the pump period. Exact expressions for the two-photon interferogram that take into account both the temporal and spatial aspects are readily derived using the formalism in Refs. [19].

Since these interference effects exist independently of

the spatial parity, they may be observed using a traditional MZI [18]. In Fig. 3, we present coincidence rates for three different settings of a PR placed in the pump beam (Fig. 2). The three coincidence interferograms displayed for the MZI are those of an even pump ( $\theta = 0$ ), an odd pump ( $\theta = \pi$ ), and a pump in an equal superposition of even and odd parity ( $\theta = \frac{\pi}{2}$ ). The coincidence rate as a function of  $\tau$  exhibits the two aforementioned features: an HOM dip (whose width is inversely related to the SPDC bandwidth) and a sinusoid with the period of the pump laser. It is obvious from the observed coincidence interferograms in Fig. 3 that the traditional MZI is oblivious to the spatial parity of the incident light.

The experimental results are altered dramatically when this traditional MZI is converted into a PS-MZI by the insertion of an SF in one of its arms. When the  $|\Psi^+\rangle$  state is generated (corresponding to an odd pump), the photons have opposite spatial parity, and hence emerge from different output ports of the PA, thereby producing a coincidence count. The two photons in the  $|\Phi^+\rangle$  state (corresponding to an even pump), on the other hand, have the same parity and hence emerge together from the same output port and do not produce a coincidence count. We expect that the  $|\Phi^+\rangle$  state will produce a minimum in the coincidence rate at  $\tau = 0$ , while the  $|\Psi^+\rangle$  state will produce a maximum. Both of these predictions are borne out by the experimental results for the PS-MZI shown in Fig. 4. The five panels correspond to different settings of the PR, varying from  $\theta = 0$  to  $\theta = \pi$ . The high-visibility HOM *dip* at  $\theta = 0$  gradually loses visibility as  $\theta$  increases, resulting in a featureless interferogram at  $\theta = \frac{\pi}{2}$ . Increasing  $\theta$  further results in the emergence of an HOM *peak*, which attains its maximal visibility at  $\theta = \pi$ .

To more explicitly demonstrate our ability to precisely control the generation of the entangled SPDC state in parity space, we have carried out an experiment in which we hold the delay fixed at  $\tau = 0$  while varying the angle  $\theta$  of the PR in the pump. The coincidence rate shown in Fig. 5 oscillates between maxima corresponding to the state  $|\Psi^+\rangle$  produced at  $\theta = \pi, 3\pi, 5\pi, \dots$  and minima at  $\theta = 0, 2\pi, 4\pi, \dots$  corresponding to the state  $|\Phi^+\rangle$ . The curve thus obtained represents five complete circumnavigations of the Poincaré sphere representing the pump's spatial parity. Confirmation of the presence of entanglement is achieved by demonstrating a Bell-inequality violation, as we have shown in Ref. [20].

In conclusion, we have demonstrated the controlled synthesis of two-photon states entangled in the parity of one dimension of their transverse spatial distribution. The prescribed states are controlled by manipulating the spatial parity of the pump, a classical parameter, and not by direct manipulation of the generated entangled photons. Furthermore, we constructed a parity-sensitive MZI by adding only one mirror to one arm of a traditional MZI, and showed that when the arms have equal path

lengths, this device acted as a parity analyzer. This seemingly insignificant change dramatically altered the behavior of the interferometer. It acquired sensitivity to spatial parity, which a traditional MZI lacks, and was used to analyze maximally entangled qubits in the spatial-parity basis. Our approach is inherently interesting from the point-of-view of quantum information processing. While each photon carries *one* polarization qubit, it has *two* transverse dimensions, and one qubit can be encoded in each. Furthermore, these two spatial-parity qubits per photon may be led to interact using simple optical arrangements. The two-photon SPDC state thus carries four parity qubits, allowing the study of hyperentanglement [21] in a straightforward manner.

*Acknowledgments*—This work was supported by a U. S. Army Research Office (ARO) Multidisciplinary University Research Initiative (MURI) Grant and by the Center for Subsurface Sensing and Imaging Systems (CenSSIS), an NSF Engineering Research Center. This work is sponsored by the National Aeronautics and Space Administration under Air Force Contract #FA8721-05-C-0002. Opinions, interpretations, recommendations and conclusions are those of the authors and are not necessarily endorsed by the United States Government. A.F.A. acknowledges the generous support and encouragement of Y. Fink and J. D. Joannopoulos.

---

\* URL: <http://www.bu.edu/qil>

- [1] D. Bouwmeester *et al.*, eds., *The Physics of Quantum Information* (Springer-Verlag, 2000).
- [2] N. Gisin *et al.*, Rev. Mod. Phys. **74**, 145 (2002); N. Gisin and R. Thew, Nature Photonics **1**, 165 (2007).
- [3] P. Walther *et al.*, Nature (London) **434**, 169 (2005); P. Kok *et al.*, Rev. Mod. Phys. **79**, 135 (2007).
- [4] P. G. Kwiat *et al.*, Phys. Rev. Lett. **75**, 4337 (1995).
- [5] I. Marcikic *et al.*, Phys. Rev. A **66**, 062308 (2002).
- [6] D. V. Strekalov *et al.*, Phys. Rev. Lett. **74**, 3600 (1995); T. B. Pittman *et al.*, Phys. Rev. A **52**, R3429 (1995); R. S. Bennink *et al.*, Phys. Rev. Lett. **92**, 033601 (2004); J. C. Howell *et al.*, *ibid.* **92**, 210403 (2004); A. F. Abouraddy *et al.*, *ibid.* **93**, 213903 (2004).
- [7] M. Fiorentino and F. N. C. Wong, Phys. Rev. Lett. **93**, 070502 (2004); L. Neves *et al.*, *ibid.* **94**, 100501 (2005); M. N. O'Sullivan-Hale *et al.*, *ibid.* **94**, 220501 (2005).
- [8] S. P. Walborn *et al.*, Phys. Rev. Lett. **90**, 143601 (2003); S. P. Walborn *et al.*, Phys. Rev. A **71**, 053812 (2005).
- [9] A. Mair *et al.*, Nature (London) **412**, 313 (2001); S. S. R. Oemrawsingh *et al.*, Phys. Rev. Lett. **95**, 240501 (2005).
- [10] Z.-B. Chen *et al.*, Phys. Rev. Lett. **88**, 040406 (2002); M. Revzen *et al.*, Phys. Rev. A **71**, 022103 (2005).
- [11] Č. Brukner *et al.*, Phys. Rev. A **68**, 062105 (2003).
- [12] A. F. Abouraddy *et al.*, Phys. Rev. A **75**, 052114 (2007).
- [13] M. J. Padgett and J. Courtial, Opt. Lett. **24**, 430 (1999).
- [14] B. E. A. Saleh and M. C. Teich, *Fundamentals of Photonics*, 2nd ed. (Wiley, 2007).
- [15] H. Sasada and M. Okamoto, Phys. Rev. A **68**, 012323 (2003); E. Mukamel *et al.*, Opt. Lett. **28**, 1317 (2003);

- B. J. Smith *et al.*, Opt. Lett. **30**, 3365 (2005).
- [16] S. Hill and W. K. Wootters, Phys. Rev. Lett. **78**, 5022 (1997); A. F. Abouraddy *et al.*, Phys. Rev. A **64**, 050101(R) (2001).
- [17] C. K. Hong *et al.*, Phys. Rev. Lett. **59**, 2044 (1987).
- [18] J. G. Rarity *et al.*, Phys. Rev. Lett. **65**, 1348 (1990); R. A. Campos *et al.*, Phys. Rev. A **42**, 4127 (1990); T. S. Larchuk *et al.*, *ibid.* **52**, 4145 (1995); K. Edamatsu *et al.*, Phys. Rev. Lett. **89**, 213601 (2002).
- [19] B. E. A. Saleh *et al.*, Phys. Rev. A **62**, 043816 (2000); M. Atatüre *et al.*, *ibid.* **66**, 023822 (2002).
- [20] T. Yarnall *et al.*, arXiv:0708.0653 [quant-ph] (2007).
- [21] J. T. Barreiro *et al.*, Phys. Rev. Lett. **95**, 260501 (2005).

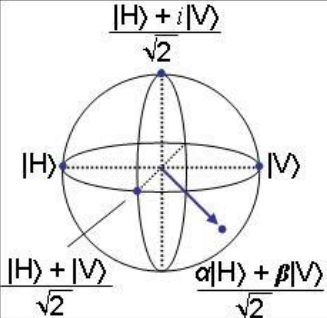
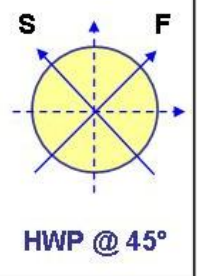
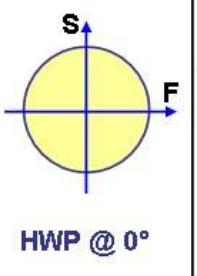
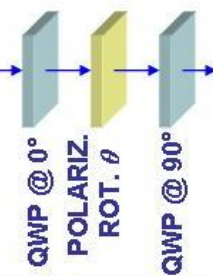
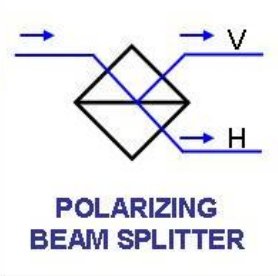
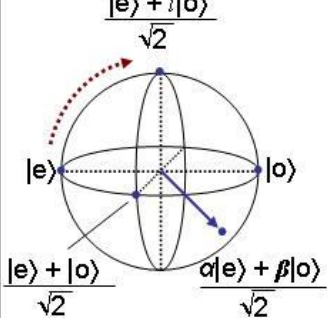
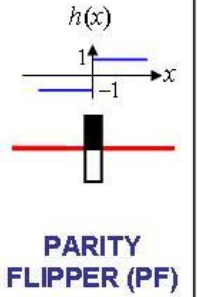
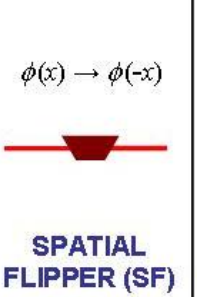
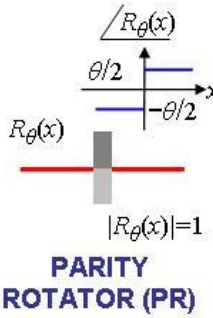
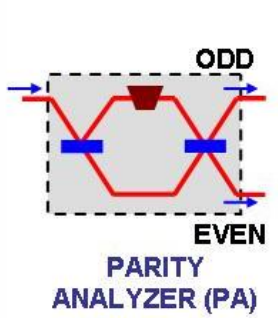
	POINCARÉ SPHERE	$\sigma_x$ $\begin{pmatrix} 0 & 1 \\ 1 & 0 \end{pmatrix}$	$\sigma_z$ $\begin{pmatrix} 1 & 0 \\ 0 & -1 \end{pmatrix}$	$R(\theta)$	PROJECTION
POLARIZATION		 HWP @ 45°	 HWP @ 0°	 QWP @ 0° POLARIZ. ROT. $\theta$ QWP @ 90°	 POLARIZING BEAM SPLITTER
SPATIAL-PARITY		 PARITY FLIPPER (PF)	 SPATIAL FLIPPER (SF)	 PARITY ROTATOR (PR)	 PARITY ANALYZER (PA)

FIG. 1: (Color online) Comparison of polarization photonic qubits and operations (first row) and their counterparts in 1D spatial parity (second row). HWP: half-wave plate; QWP: quarter-wave plate; H, V: horizontal and vertical polarization; S, F: slow and fast axes of the wave plate;  $R(\theta)$ : rotation operator;  $\sigma_x, \sigma_z$ : Pauli operators.

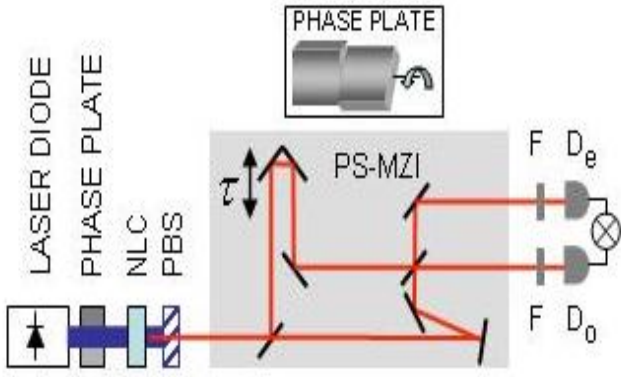


FIG. 2: (Color online) Schematic of the experimental arrangement. NLC: nonlinear crystal; PBS: polarizing beam splitter; F: interference filter; D: detector;  $\otimes$ : coincidence circuit. The PS-MZI serves as a parity analyzer. The inset shows the construction of the phase plate (parity rotator) placed in the path of the pump. It comprises two glass microscope slides, abutted at the center of the pump beam, that can be tilted with respect to each other.

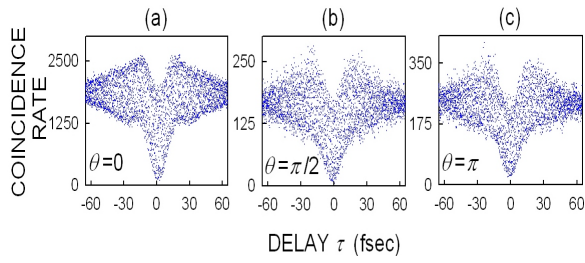


FIG. 3: (Color online) Observed coincidence rate from a traditional MZI for three different settings of a parity rotator placed in the pump: (a)  $\theta = 0$  (even pump), (b)  $\theta = \frac{\pi}{2}$  (equal superposition of even and odd), and (c)  $\theta = \pi$  (odd pump).

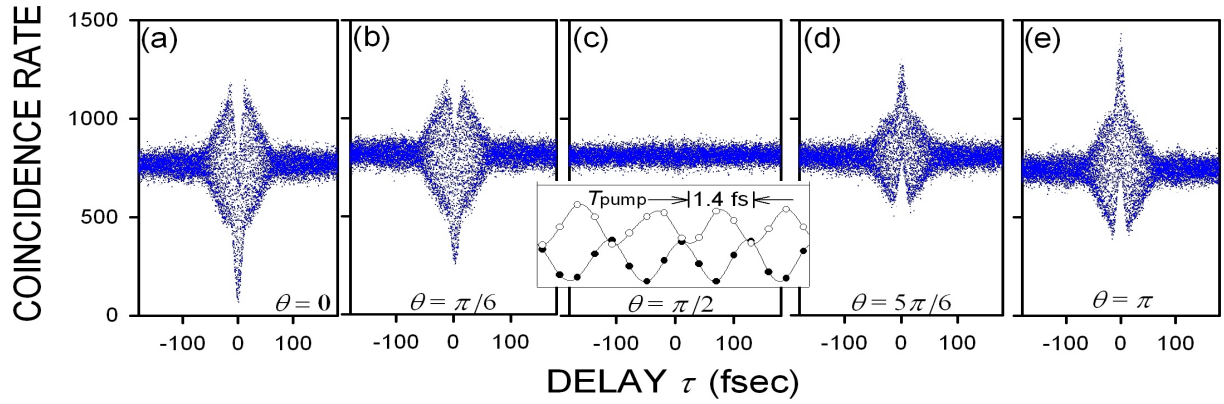


FIG. 4: (Color online) Coincidence rate at the output of a PS-MZI for different settings of the parity rotator placed in the pump beam. The five settings are (a)  $\theta = 0$  (pump is even), (b)  $\theta = \frac{\pi}{6}$ , (c)  $\theta = \frac{\pi}{2}$  (equal superposition of even and odd), (d)  $\theta = \frac{5\pi}{6}$ , and (e)  $\theta = \pi$  (pump is odd). The inset shows oscillation at the pump period  $T_{\text{pump}}$  for panels (a) (full circles) and (e) (open circles) near  $\tau = 0$ . The two curves, which are spline fits, are  $180^\circ$  out of phase, as expected.

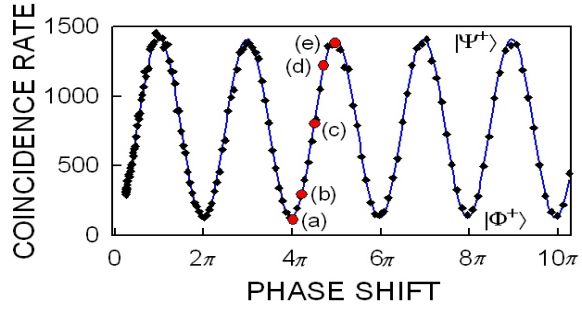


FIG. 5: (Color online) Coincidence rate at  $\tau = 0$  of the PS-MZI as the parity of the pump is continuously varied over the range  $0 < \theta < 10\pi$ . The diamonds represent experimental data; the solid curve is a theoretical fit. The five circles labeled (a)–(e) correspond to the five settings used in the panels of Fig. 4.